Dynamics and coherence of a multimode semiconductor laser with optical feedback in an intermediate-length external-cavity regime

C. Serrat, S. Prins,* and R. Vilaseca
Departament de Física i Enginyeria Nuclear, Universitat Politècnica de Catalunya, Colom 1, E-08222 Terrassa, Spain
(Received 26 February 2003; published 4 November 2003)

We use a traveling-wave numerical model of the temporal dynamics in semiconductor lasers to investigate the dynamics and coherence properties of a multimode semiconductor laser subject to optical feedback. Considering an external cavity of intermediate length, we have observed features characteristic of the so-called *short-cavity* regime in a region where the relaxation oscillations frequency is larger than the external-cavity frequency. The time scales of the dynamics are controlled in this case by the strength of the optical feedback. We have examined the coherence properties of the multimode emission and have studied how the coherence time is reduced as the laser becomes more multimode.

DOI: 10.1103/PhysRevA.68.053804 PACS number(s): 42.65.Sf, 05.45.Jn, 42.55.Px

I. INTRODUCTION

Semiconductor lasers play a central role in the growing world of optoelectronic technologies. Intense research activity in recent years has been focused on the effect of optical feedback in the dynamics of these lasers. In this context, several studies have focused their attention on the multimode behavior of semiconductor lasers, since many practical applications normally use semiconductor lasers operating in several longitudinal modes simultaneously [1]. On the other hand, delayed dynamical systems have become a broad interdisciplinary subject, since this type of systems appear in many different fields of science [2], semiconductor lasers constituting an excellent tool to investigate their behavior.

In the context of the optoelectronic industry, relatively short external cavities are relevant for many applications (e.g., fiber couplers or compact discs). In a recent study [3], it was shown that the characteristics of the dynamics of a semiconductor laser subject to optical feedback depend strongly on the length of the external cavity. In particular, Heil *et al.* [3] showed that the dynamical behavior of the system is governed by one of the two basic frequencies, namely, the relaxation oscillations frequency ν_{RO} in the case of the so-called long-cavity regime (LCR), and the external-cavity frequency ν_{EC} in the case of the so-called short-cavity regime (SCR). Indeed, for long external cavities ($\nu_{RO} \gg \nu_{EC}$), the behavior of the system is characterized by irregular fast pulses at $\sim \nu_{RO}$, while the dynamics show regular pulses at ν_{EC} in the case of short external cavities ($\nu_{RO} \ll \nu_{EC}$). To our knowledge, however, no study of the regime corresponding to cavities of intermediate length has been performed, so that the main features characterizing the laser behavior in such conditions are not known.

In the present paper, we analyze the influence of multilongitudinal-mode emission on the dynamics of a semiconductor laser with an external cavity of length of the order of 12 cm, which is intermediate between the LCR and SCR cases. Due to the length of the external cavity that we consider, the ratio ν_{RO}/ν_{EC} is reversed as the injection current is varied, with $\nu_{RO}/\nu_{EC}<1$ near the lasing threshold, and $\nu_{RO}/\nu_{EC}>1$ for larger values of the injection current. Our contribution consists in the study of the region around twice the lasing threshold, which is interesting from an applied point of view for potential applications in chaotic secure communications [5]. By thus fixing the injection current at twice the lasing threshold, we obtain, for the case considered in the present study, $\nu_{RO}\approx 2.6$ GHz and $\nu_{EC}\approx 1.2$ GHz. In such conditions, we will show that the system switches from dynamics dominated by ν_{RO} to dynamics that include pulses at ν_{EC} by only increasing the feedback strength. Additionally, we also analyze in this paper the temporal coherence of the emission, as a function of several laser parameters, by means of the visibility function. As it will be discussed in detail, we observe how the coherence time is degraded as the laser becomes more multimode.

In Sec. II we describe the system and the procedure used for numerical integration. In Sec. III our main results are presented and discussed and in Sec. IV the main conclusions are summarized.

II. MODEL AND NUMERICAL INTEGRATION

We use a traveling-wave model of coupled partial differential equations recently derived by White *et al.* [4], which

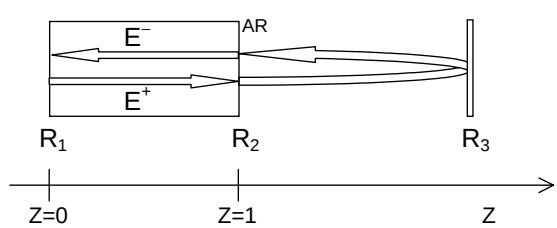

FIG. 1. Illustration of the laser cavity. The mirror effective reflectivities are R_1, R_2, and R_3. Inside the cavity, the forward and backward propagating fields are E^+ and E^-, respectively. The mirror with reflectivity R_2 is antireflection coated (AR) for beams coming from the external mirror R_3.

*Permanent address: Vrije Universiteit Brussel, Department of Applied Physics and Photonics, Pleinlaan 2, B-1050 Brussels, Belgium.

describes the laser field as it propagates in the laser cavity by taking into account the longitudinal dependence of the field and the carriers. It consists of a set of partial differential equations which, in their adimensional form, are given by

$$\frac{\partial E^{\pm}}{\partial t} \pm \frac{\partial E^{\pm}}{\partial z} = \kappa\left[(N-1)\left(1+G_d\frac{\partial^2}{\partial z^2}\right) - i\alpha N - \gamma_{int}\right]E^{\pm}, \tag{1}$$

$$\frac{\partial N}{\partial t} = J - \gamma N - (N-1)[|E^{+}|^2 + |E^{-}|^2] \tag{2}$$

together with boundary conditions given by

$$E^{+}(0,t) = \sqrt{R_1}E^{-}(0,t), \tag{3}$$

$$E^{-}(1,t) = \sqrt{R_2}E^{+}(1,t) + \sqrt{(1-R_2)R_3}E^{+}(1,t-\tau_{EC}), \tag{4}$$

which determine the longitudinal-mode complex wave vectors and allow to derive the cavity modes of the laser resonator, the loss due to the cavity mirrors, and the threshold condition [6]. $E^{\pm}$ are the slowly varying complex amplitudes of the forward E^{+} and backward E^{-} intracavity propagating fields, and N is the carrier density. The parameter κ is given by $(1/2)L_c\Gamma a N_0$, where L_c is the solitary laser effective cavity length, Γ is the lateral confinement factor, a is the gain constant, and N_0 is the carrier density at transparency. G_d is the gain dispersion constant modeling the gain bandwidth $\Delta\nu_g \approx c/(2\pi n L_c\sqrt{G_d})$, where c is the speed of light in vacuum and n is the base refractive index of the gain material [4]. α is the linewidth enhancement factor, the internal losses are given by γ_{int}, the carrier damping rate is γ, and the pumping parameter (normalized injection current) is J. $R_{1,2,3}$ are the facet effective reflectivities, with R_3 corresponding to the external mirror (see Fig. 1), and τ_{EC} is the external cavity round-trip time. Note that in Eq. (4) we have neglected multiple reflections between the external mirror R_3

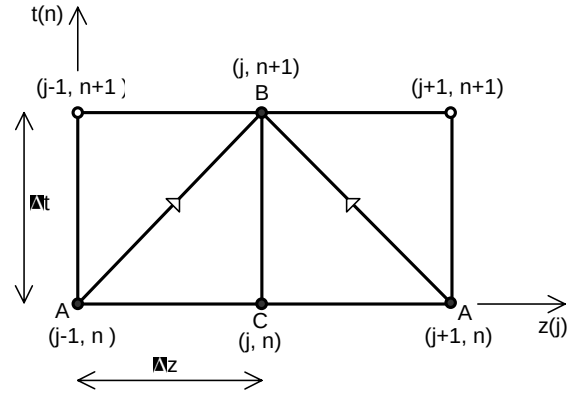

FIG. 2. Finite-difference grid for the numerical solution of the system.

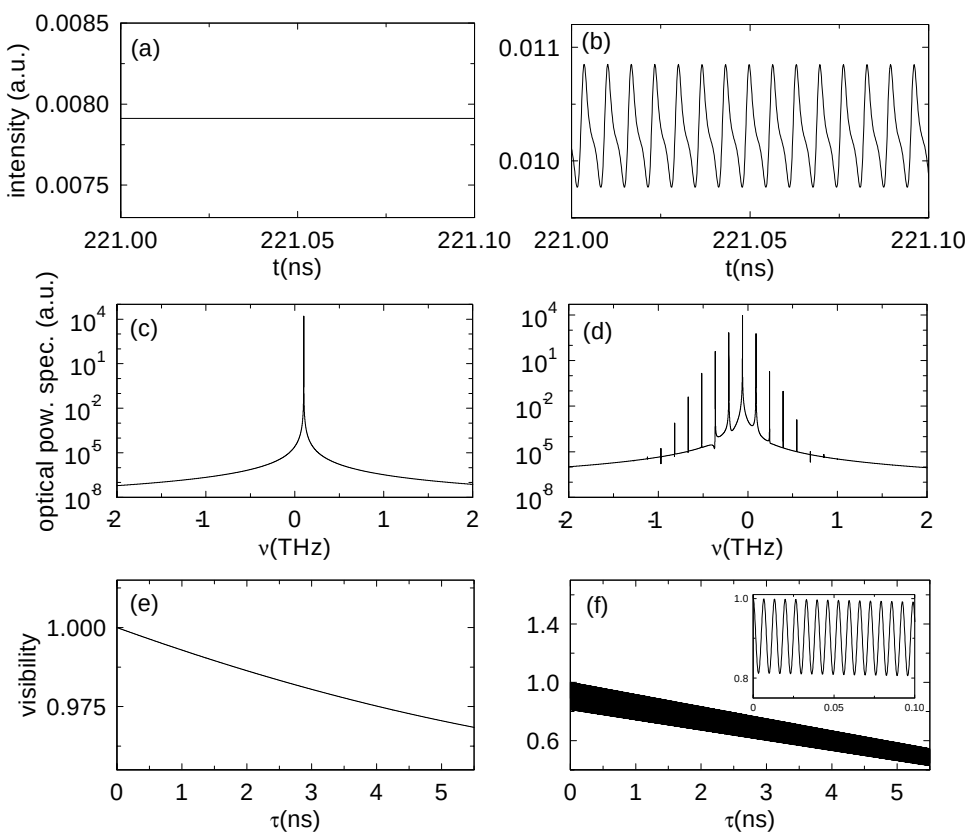

FIG. 3. Simulations for the solitary laser ($R_3=0$). Evolution of the total intracavity field intensity ($|E|^2$) (a),(b), optical power spectrum (c),(d), and visibility function (e),(f) for $G_d=2\times10^{-4}$ (a),(c),(e) and $G_d=4\times10^{-6}$ (b),(d),(f). The total intracavity electric field $[E(t,z)=E^{+}(t,z)+E^{-}(t,z)]$ is measured at $z=0$.

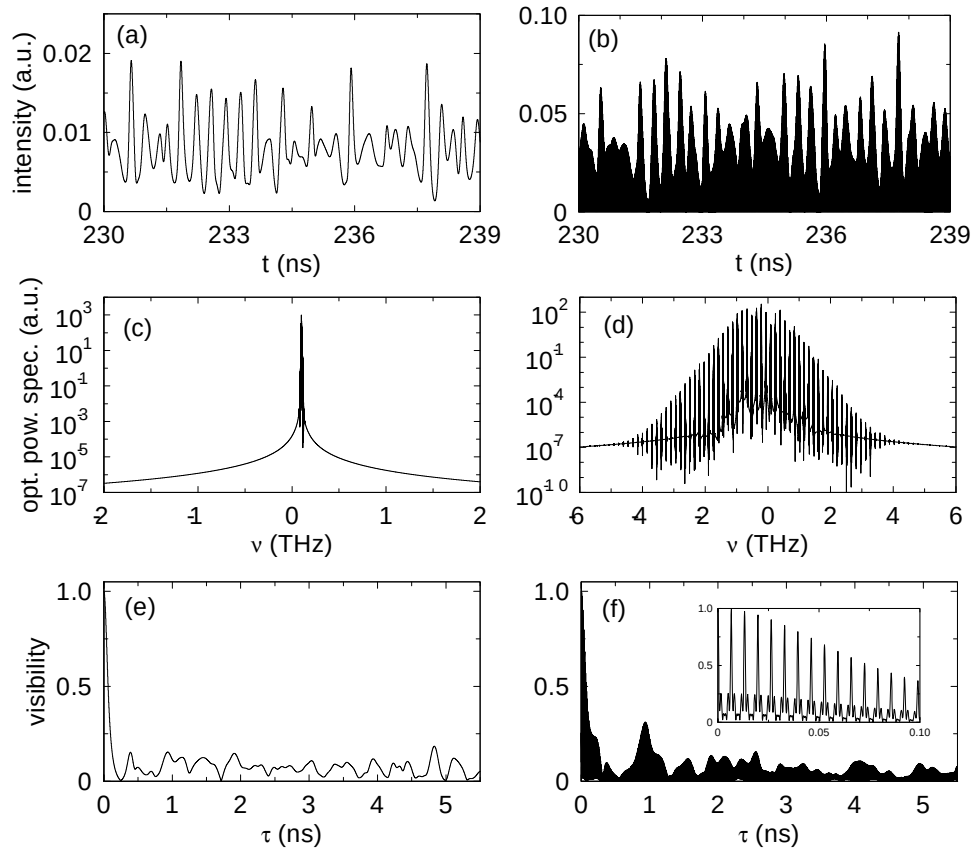

FIG. 4. Simulations for $R_3=0.0002$. Evolution of the total intracavity field intensity ($|E|^2$) (a),(b), optical power spectrum (c),(d), and visibility function (e),(f) for $G_d=2\times10^{-4}$ (a),(c),(e) and $G_d=4\times10^{-6}$ (b),(d),(f).

and the laser cavity facet R_2, which is reasonable provided the cavity facet R_2 is antireflection coated for beams coming from the external mirror. In Eqs. (1)–(4), the spatial and time variables are normalized to the length of the cavity and the one-passage time, respectively, and the carrier density is normalized to its value at transparency. Note also that the model does not include noise sources, which is consistent in the dynamical regions that are of interest for the present study, as it will be discussed in the following section. The solitary laser effective cavity length in our simulations is $L_c=275$ μm, which results in a cavity round-trip time as $\tau_c=6.6$ ps for $n=3.6$, while the value of the external cavity has been chosen as $L_{EC}=12.3$ cm, giving $\tau_{EC}=820$ ps. The other parameter values used in our study are typical for semiconductor lasers: $\Gamma=0.032$, $a=2\times10^{-20}$ m^2, and $N_0=10^{24}$ m^{-3}, which give $\kappa=0.088$, $\alpha=4$, $\gamma_{int}=0.79$, $\gamma=0.0049$, $R_1=0.95$, and $R_2=0.3$.

The system has been numerically integrated by using a finite difference integration scheme which is similar to that described in Ref. [4], but which allows to solve the whole problem explicitly. Indeed, the total derivatives which appear on the left-hand side of Eq. (1) are expressed in terms of directional derivatives in the t, z plane, with directions given by the unit vectors $(1/\sqrt{2},\pm1/\sqrt{2})$

$$\frac{dE^{\pm}}{ds}=\frac{1}{\sqrt{2}}[\mathcal{N}(N)+\mathcal{G}(N)]E^{\pm}, \tag{5}$$

with s being a length in the direction of the unit vector. As in Ref. [4], the right-hand side in Eq. (5) has been split into the following two operators:

$$\mathcal{N}(N)=\kappa[(N-1)-i\alpha N-\gamma_{int}], \tag{6}$$

$$\mathcal{G}(N)=\kappa(N-1)G_d\frac{\partial^2}{\partial z^2}. \tag{7}$$

We then discretize Eq. (5) together with Eqs. (2)–(4), and solve both parts in Eq. (5) explicitly. Assuming that $\Delta t=\Delta z=\Delta s/\sqrt{2}\equiv\Delta h$, Eq. (5) is integrated from $A\equiv(z_{j\mp1},t_n)$ to $B\equiv(z_j,t_{n+1})$ (see Fig. 2), while Eq. (2) is integrated from $C\equiv(z_j,t_n)$ to $B\equiv(z_j,t_{n+1})$. The corresponding discretized equations read

$$E_j^{\pm n+1}=[1+\Delta h\mathcal{G}(N)_{j\mp1}^n]\exp[\Delta h\mathcal{N}(N)_{j\mp1}^n]E_{j\mp1}^{\pm n}, \tag{8}$$

$$N_j^{n+1}=N_j^n+\Delta t[J-\gamma N_j^n-(N_j^n-1)(|E_j^{+n}|^2+|E_j^{-n}|^2)]. \tag{9}$$

The solution of the first integration step in Eq. (8), which involves $\mathcal{N}(N)$ and gives $E_j^{\pm n+1}$, is used as the initial value in the second step, i.e., it is taken as $E_{j\mp1}^{\pm n}$. We use integration increments as $\Delta z=\Delta t=1/300$, which correspond to a spatial step of 0.9 μm and a temporal step of 11 fs. As initial conditions, we use a random distribution for the field at each

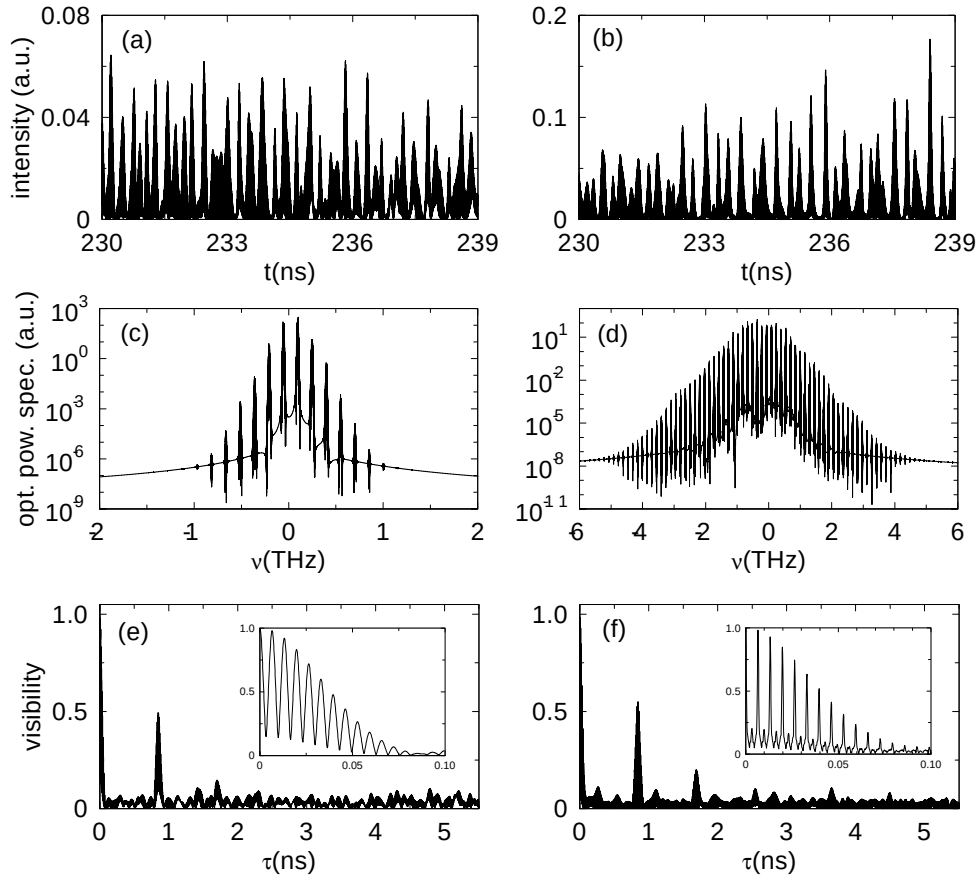

FIG. 5. Simulations for $R_3=0.004$. Evolution of the total intracavity field intensity ($|E|^2$) (a),(b), optical power spectrum (c),(d), and visibility function (e),(f) for $G_d=2\times10^{-4}$ (a),(c),(e), and $G_d=4\times10^{-6}$ (b),(d),(f).

point of the spatial grid, with values between 0 and 0.1, and we take 0.95 as the initial value for the carrier density variables.

III. RESULTS AND DISCUSSION

As it has been mentioned in the Introduction, we have centered our study at a value of the injection current of approximately twice the lasing threshold ($J=0.05\approx2J_{thr}$). For a given cavity configuration (L_c,L_{EC},R_1,R_2), the number of modes excited at a given value of the injection current is governed by the material gain dispersion G_d together with the amount of feedback involved R_3. In order to investigate the properties of the emission due to the number of longitudinal modes involved, we have analyzed the system for two different values of the gain dispersion: $G_d=2\times10^{-4}$, which results in single-mode emission in the case of the solitary laser [see Fig. 3(c)] and gives a gain-bandwidth as $\Delta\nu_g\approx3.4$ THz, and $G_d=4\times10^{-6}$, which results in multimode emission [see Fig. 3(d)] and gives a gain bandwidth as $\Delta\nu_g\approx24.1$ THz. Note that the study of this last large value of the gain bandwidth may be important for optical communication applications, where a nearly constant gain is needed over the bandwidth of, for instance, a multichannel system [6].

Figure 3 shows the calculations performed in the case of the solitary laser, i.e., without optical feedback ($R_3=0$). Figure 3(a),(c),(e) show the results corresponding to $G_d=2\times10^{-4}$ and Figs. 3(b),(d),(f) are the results obtained for $G_d=4\times10^{-6}$. The field evolves in a steady state in the case of single-mode emission [Fig. 3(a)], while very fast dynamics appear when several longitudinal modes are excited [Fig. 3(b)]. Those very fast dynamics have a time scale of a few picoseconds, which corresponds to the time scale of the round-trip time in the solitary laser cavity τ_c, or, in other words, to the free spectral range of the solitary laser (≈151 GHz). As it can be observed comparing Fig. 3(c) with Fig. 3(d), different longitudinal modes can be selected near the peak gain ($\nu=0$). This effect is due to the large difference between the gain bandwidth and the separation in frequency between the longitudinal modes, which results in a comparable gain for the modes close to $\nu=0$. The excited mode is then selected by the particular initial conditions of the system, which in our simulations are taken randomly as it has been pointed out above.

In order to investigate the lasing coherence properties, we compute the visibility function, which is defined as

$$V(\tau)=|G_E(\tau)|, \tag{10}$$

where τ is a delay time and $G_E(\tau)$ is the normalized two-point time autocorrelation function of the total intracavity electric field $E(t)=E^+(t,0)+E^-(t,0)$ at $z=0$, which is given by

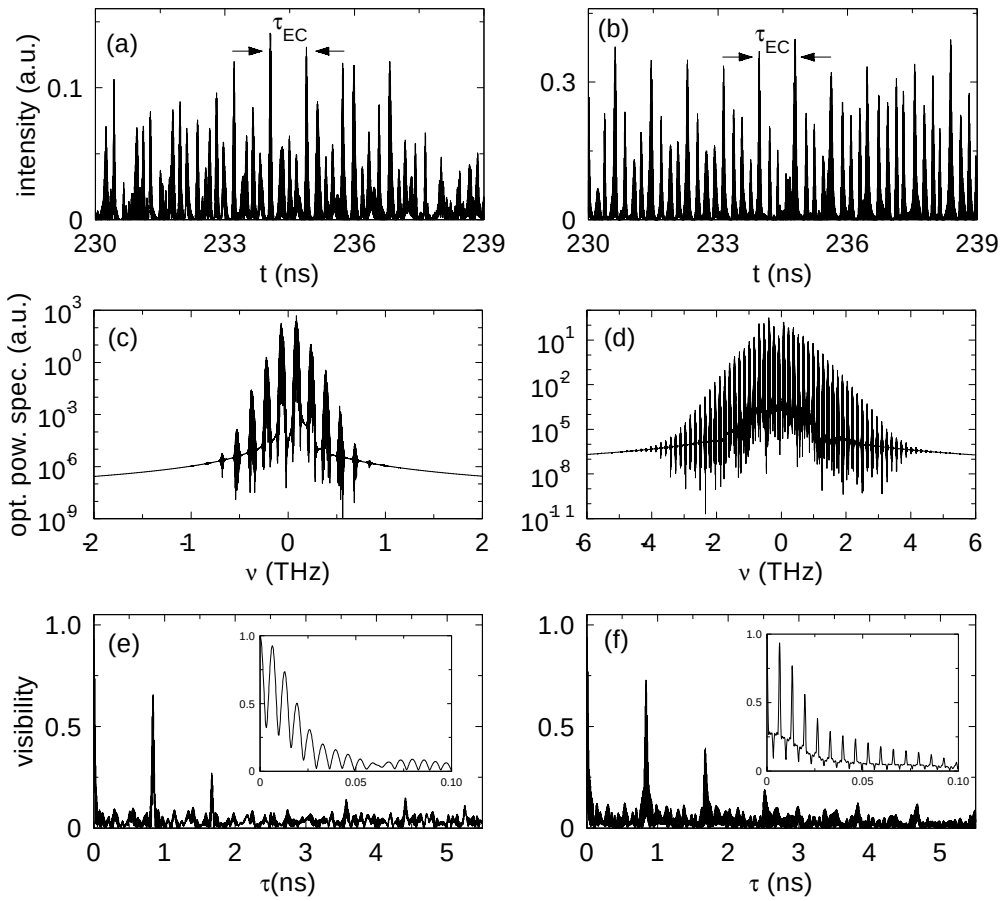

FIG. 6. Simulations for $R_3=0.03$. Evolution of the total intracavity field intensity ($|E|^2$) (a),(b), optical power spectrum (c),(d) and visibility function (e),(f) for $G_d=2\times10^{-4}$ (a),(c),(e) and $G_d=4\times10^{-6}$ (b),(d),(f).

$$G_E(\tau)=\frac{\langle E(t)E^*(t-\tau)\rangle}{\langle|E(t)|^2\rangle}. \tag{11}$$

In this last expression, $\langle\ \rangle$ implies an averaging over t, which is treated as an ensemble average by interpreting t as an index labeling the elements of the ensemble, so that an averaging over the fluctuations of the phase and the amplitude of the optical field is achieved. $V(\tau)$ gives a quantitative measurement of the temporal coherence of the lasing emission. Note that for perfectly monochromatic light $V(\tau)=1$ for all τ. As it can be observed from Figs. 3(e),(f), in the case of the solitary laser ($R_3=0$) we obtain a high degree of coherence in both cases, which is expected since no quantum-noise sources are included in the equations. Interestingly, Fig. 3(f) shows the fingerprint of the multimode emission on the visibility function, which oscillates at the same frequency as the intensity signal [Fig. 3(b)]. We note here that we employ the Wiener-Kintchine theorem in order to numerically calculate the visibility function, which states that the optical power spectrum is the Fourier transform of the two-point time autocorrelation function

$$G_E(\omega)=\langle|E(\omega)|^2\rangle. \tag{12}$$

We next discuss the results of the influence of optical feedback on the solitary laser behavior. Figures 4–6 show the intensity versus time traces (a),(b), optical power spectra (c),(d) and visibility functions (e),(f) for $G_d=2\times10^{-4}$ (a),(c),(e), and $G_d=4\times10^{-6}$ (b,d,f), computed at increasing values of optical feedback, as indicated. Figure 4 shows that a small value of feedback ($R_3=0.0002$) is sufficient to induce sustained relaxation oscillations in the system, which appear as oscillations in the intensity evolution in the case of single-mode emission [Fig. 4(a)] and as a modulation of the previously discussed very fast dynamics in the case of multimode emission [Fig. 4(b)]. Focusing on the visibility curves [Figs. 4(e),(f)], we observe that they fall to values near zero already at relatively small delay times. Here We note that, sufficiently above the lasing threshold, and thus in the region of our study ($J\approx2J_{thr}$), the fluctuations induced in the system due to moderate feedback levels are stronger than those corresponding to spontaneous emission noise [7], and hence neglecting noise sources in the present calculations is a reasonable approximation.

As a consequence of increasing the feedback strength [see Figs. 5 and 6], the semiconductor laser exhibits multimode behavior for both $G_d=2\times10^{-4}$ and $G_d=4\times10^{-6}$, although many more modes are excited in the case of the broader gain bandwidth. Figures 5 and 6 show several important features.

(i) The appearance of intensity very fast dynamics ($\sim$ps) due to the excitation of some longitudinal modes in the case of $G_d=2\times10^{-4}$ [see Figs. 5(a) and 6(a)].

(ii) The modulation of the very fast dynamics in a lower time scale, showing an irregular pulsed-type behavior in all cases [see Figs. 5(a),(b) and 6(a),(b)],

(iii) For $R_3=0.004$ (Fig. 5), the time scale of such pulses, as in Fig. 4, is of the order of the relaxation oscillations of the system, which is a characteristic of the LCR. For higher values of feedback ($R_3 \gtrsim 0.01$), however, a second time scale, which corresponds to the external-cavity round-trip time τ_{EC}, appears in the dynamics [see Fig. 6(a),(b)]. The dynamical behavior of the system in this region thus involves irregular pulses at $\nu_{RO} \approx$ 2.6 GHz and pulses at $\nu_{EC} \approx 1.2$ GHz. We attribute this effect to the particular length of the external cavity that we have studied. Comparing Fig. 6 (a) with Fig. 6(b) we observe that the pulses at ν_{EC} are more regular in the case of the broader gain bandwidth.

(iv) The linewidth of the individual spectral components increases as the feedback strength is increased [see Figs. 5(c),(d) and 6(c),(d)], and hence a developing collapse of the coherence appears in each mode, as it could have been expected since this is the behavior commonly observed in the single-mode case [8]. We also note that those individual peaks have an internal structure (not shown here) which includes other spectral components resolved at frequency scales much smaller than the free spectral range of the solitary laser—such as the relaxation oscillations and the external-cavity frequencies.

(v) The visibility function shows fast *dynamics*, which are linked to the intensity dynamics, with oscillations in time scales that comprise the cavity round-trip time and the relaxation oscillations. Furthermore, sharp peaks at the external-cavity round-trip time, and at multiples of it, appear in the visibility function, which become stronger as the feedback strength is increased [see Figs. 5(e),(f) and 6(e),(f)].

In order to have a further description of the temporal coherence properties of the multimode lasing emission in this region, we evaluate the overall coherence time, which is defined as

$$\tau_{coh}=\int_{-\infty}^{+\infty}|V(\tau)|^2 d\tau=2\int_{0}^{+\infty}|V(\tau)|^2 d\tau. \qquad (13)$$

The coherence time τ_{coh} provides an estimation of the delay time at which the visibility $V(\tau)$ first reaches a value close to zero [9]. We want to have a qualitative idea of the behavior of τ_{coh} as a function of the gain dispersion parameter G_d and the amount of feedback involved in the system (R_3). We cannot, however, pretend quantitative results, since apart from the inherent errors in the evaluation of τ_{coh} due to the finite time traces that we use in the numerical calculations, the results obtained for τ_{coh} can only be trusted in the range $10^{-4} \lesssim R_3 \lesssim 0.05$. Indeed, for $R_3 \lesssim 10^{-4}$, the visibility function stays at values close to one for all delay times τ as it has been mentioned above [see Figs. 3(e),(f)], a fact which is due to the absence of noise sources in the equations. An estimation of the Schawlow-Townes (quantum limited) coherence time corresponding to a single-mode laser, featuring the configuration that we are studying, gives roughly 0.6 ns at $J \approx 2J_{thr}$, and hence our calculations have a physical meaning for $\tau_{coh} \lesssim 0.6$ ns. We have not attempted either to study the regime of large feedback ($R_3 \gtrsim 0.05$), in which the emission reaches high degrees of coherence due to the amount of light that is fed back to the laser cavity. Figure 7(a) shows the computed coherence time as a function of the feedback strength R_3 for two different values of the gain dispersion G_d, as indicated. The fluctuations in that figure are due to the finite time traces used in the calculations, as it has been noted above. We observe that the value of τ_{coh} is around 0.07 ns for a wide range of feedback strength ($5\times10^{-4} \lesssim R_3 \lesssim 0.01$) in the case of the larger gain dispersion $G_d = 2\times10^{-4}$, while it drops to roughly half that value in the case of the smaller gain dispersion $G_d = 4\times10^{-6}$. We hence observe how the temporal coherence of the emitted light is degraded when a larger number of longitudinal modes is involved in the field. This effect is also shown in Fig. 7(b), where the coherence time τ_{coh} has been computed as a function of the gain dispersion G_d for two different values of the feedback strength ($R_3=0.001$ and $R_3=0.01$), although differences due to the amount of feedback cannot be appreciated in our calculations.

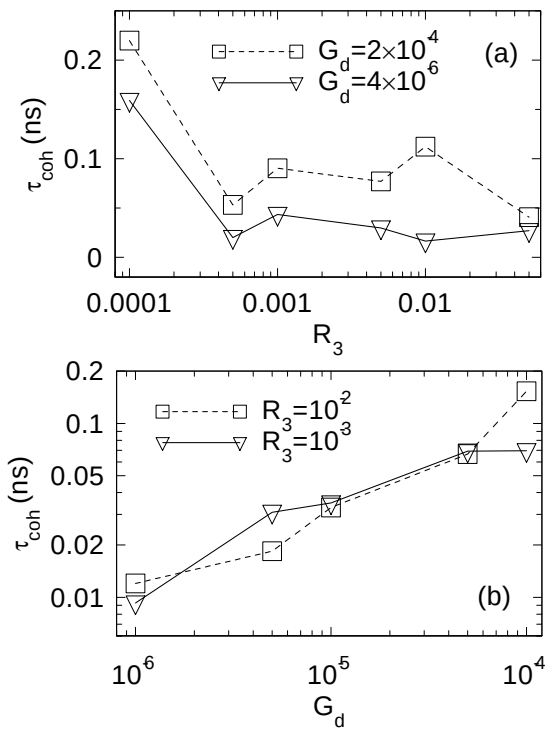

FIG. 7. Coherence time as a function of the feedback strength (R_3) for different values of the gain dispersion G_d as indicated in (a). Coherence time as a function of the gain dispersion G_d for different values of the feedback strength R_3 as indicated in (b). The lines are a guide to the eye.

IV. CONCLUSIONS

We have numerically integrated a well established deterministic model to study the dynamics of a multi-mode semiconductor laser subject to optical feedback in conditions of a fixed intermediate-length external-cavity configuration. We have centered our investigation on the influence of the number of longitudinal modes involved in the dynamics. A wide

range of feedback strengths has been covered, although our study has been limited to a value of the injection current as twice the lasing threshold. At moderate feedback levels, we have observed the appearance of pulses at ν_{EC} in a region where $\nu_{RO} > \nu_{EC}$. The temporal coherence properties of the emission have been examined by studying the visibility function and the overall coherence time. We have observed rich behaviors of the visibility function due to the interplay of multimode emission and optical feedback. We have carried out a qualitative study of the influence of the gain bandwidth and the feedback strength on the coherence time, showing how the temporal coherence is degraded as the number of modes in the field increases. The accuracy of the results in calculating the coherence time are strongly dependent, however, on the time interval used in the fast Fourier transform (FFT) algorithm. Indeed, due to computing capabilities, we are able to use a maximum of 23 ns in the (FFT) algorithm, which is not enough for the coherence time τ_{coh} to converge in the region that we have studied. Hence, we are only able to provide a qualitative study of the behavior of the coherence time; this qualitative behavior remains, nevertheless, for different realizations of the simulations and also when using shorter time traces in the FFT algorithm. Finally, we want to point out that we have investigated a particular length of the external cavity, and thus other studies are required in order to have a more complete description of the phenomena observed here.

ACKNOWLEDGMENTS

This research was financially supported by (''Contrato de Incorporación de Doctores y Tecnólogos'') from the ''Dirección General de Educación Superior e Investigación Científica'' (DGESIC), Project Nos. PB98-0935-C03-01 and BFM2002-04369-C04-03 (DGESIC), Project No. 2001SGR0023 (''Generalitat de Catalunya''), and the ''Center Europeu de Parallelisme de Barcelona'' (CEPBA). S.P. acknowledges support from the ERASMUS-SOCRATES Program.

[1] J. Mørk, B. Tromborg, and P.L. Christiansen, IEEE J. Quantum Electron. **24**, 123 (1988); A.T. Ryan, G.P. Agrawal, G.R. Gray, and E.C. Gage, *ibid.* **30**, 668 (1994); M. Homar, J.V. Moloney, and M. San Miguel, *ibid.* **32**, 553 (1996); D.W. Sukow, T. Heil, I. Fisher, A. Gavrielides, A. Hohl-AbiChedid, and W. Elsäßer, Phys. Rev. A **60**, 667 (1999); G. Huyet, J.K. White, A.J. Kent, S.P. Hegarty, J.V. Moloney, and J.G. McInerney, *ibid.* **60**, 1534 (1999); T.W. Carr, D. Pieroux, and P. Mandel, *ibid.* **63**, 033817 (2001); F. Rogister, P. Megret, O. Deparis, and M. Blondel, *ibid.* **62**, 061803(R) (2001); J.M. Buldú, F. Rogister, J. Trull, C. Serrat, M.C. Torrent, J. García-Ojalvo, and C.R. Mirasso, J. Opt. B: Quantum Semiclassical Opt. **4**, 415 (2002).

[2] Z.H. Wang, H.Y. Hu, and W. Zaihua, *Dynamics of Controlled Mechanical Systems with Delayed Feedback*, (Springer-Verlag, Berlin, 2002).

[3] T. Heil, I. Fisher, and W. Elsäßer, Phys. Rev. Lett. **87**, 243901 (2001).

[4] J.K. White, J.V. Moloney, A. Gavrieldes, V. Kovanis, A. Hohl, and R. Kalmus, IEEE J. Quantum Electron. **34**, 1469 (1998).

[5] L. Rahman, G. Li, and F. Tian, Opt. Commun. **138**, 91 (1997); P.S. Spencer, C.R. Mirasso, P. Colet, and K.A. Shore, IEEE J. Quantum Electron. **34**, 1673 (1998); J.K. White and J.V. Moloney, Phys. Rev. A **59**, 2422 (1999); A. Uchida, Y. Liu, I. Fisher, P. Davis, and T. Aida, *ibid.* **64**, 023801 (2001).

[6] G.P. Agrawal and N.K. Dutta, *Semiconductor Lasers* (Kluwer Academic, Dordrecht, MA, 2001).

[7] J.S. Cohen and D. Lenstra, IEEE J. Quantum Electron. **25**, 1143 (1989); J.S. Cohen, F. Wittgrefe, M.D. Hoogerland, and J.P. Woerdman, *ibid.* **26**, 982 (1990).

[8] D. Lenstra, B.H. Verbeek, and J. den Boef, IEEE J. Quantum Electron. **21**, 674 (1985).

[9] L. Mandel and E. Wolf, *Optical Coherence and Quantum Optics*, (Cambridge University Press, Cambridge, 1995).